Journal of Proteomics 244 (2021) 104276

Contents lists available at ScienceDirect

Journal of Proteomics

journal homepage: www.elsevier.com/locate/jprot

Proteome remodeling in the *Mycobacterium tuberculosis* PknG knockout: Molecular evidence for the role of this kinase in cell envelope biogenesis and hypoxia response

Analía Lima [a], Alejandro Leyva [a], Bernardina Rivera [a], María Magdalena Portela [a,h], Magdalena Gil [a,1], Alessandro Cascioferro [b,2], María-Natalia Lisa [c,d], Annemarie Wehenkel [c], Marco Bellinzoni [c], Paulo C. Carvalho [e], Carlos Batthyány [f], María N. Alvarez [g], Roland Brosch [b], Pedro M. Alzari [c], Rosario Durán [a,*]

[a] *Institut Pasteur de Montevideo & Instituto de Investigaciones Biológicas Clemente Estable, Unidad de Bioquímica y Proteómica Analíticas, Montevideo, Uruguay*
[b] *Institut Pasteur, Unit for Integrated Mycobacterial Pathogenomics, CNRS UMR 3525, Paris 75015, France*
[c] *Structural Microbiology Unit, Institut Pasteur, CNRS UMR 3528, Université de Paris, F-75015 Paris, France*
[d] *Instituto de Biología Molecular y Celular de Rosario (IBR, CONICET-UNR), Ocampo y Esmeralda, Rosario S2002LRK, Argentina*
[e] *Carlos Chagas Institute, Structural and Computational Proteomics, Fiocruz-Paraná, Brazil*
[f] *Institut Pasteur de Montevideo, Vascular Biology and Drug Development Laboratory, Uruguay*
[g] *Universidad de la República, Facultad de Medicina, CEINBIO, Departamento de Bioquímica, Uruguay*
[h] *Universidad de la República, Facultad de Ciencias, Uruguay*

ARTICLE INFO

Keywords:
Mycobacterium tuberculosis
Serine/Threonine protein kinase
PknG
Mas
Msl3
Hypoxia
Hrp-1

ABSTRACT

Mycobacterium tuberculosis, the etiological agent of tuberculosis, is among the deadliest human pathogens. One of *M. tuberculosis*'s pathogenic hallmarks is its ability to persist in a dormant state in the host. Thus, this pathogen has developed mechanisms to withstand stressful conditions found in the human host. Particularly, the Ser/Thr-protein kinase PknG has gained relevance since it regulates nitrogen metabolism and facilitates bacterial survival inside macrophages. Nevertheless, the molecular mechanisms underlying these effects are far from being elucidated. To further investigate these issues, we performed quantitative proteomic analyses of protein extracts from *M. tuberculosis* H37Rv and a mutant lacking *pknG*. We found that in the absence of PknG the mycobacterial proteome was remodeled since 5.7% of the proteins encoded by *M. tuberculosis* presented significant changes in its relative abundance compared with the wild-type. The main biological processes affected by *pknG* deletion were cell envelope components biosynthesis and response to hypoxia. Thirteen DosR-regulated proteins were underrepresented in the *pknG* deletion mutant, including Hrp-1, which was 12.5-fold decreased according to Parallel Reaction Monitoring experiments. Altogether, our results allow us to postulate that PknG regulation of bacterial adaptation to stress conditions might be an important mechanism underlying its reported effect on intracellular bacterial survival.

Significance: PknG is a Ser/Thr kinase from *Mycobacterium tuberculosis* with key roles in bacterial metabolism and bacterial survival within the host. However, at present the molecular mechanisms underlying these functions remain largely unknown. In this work, we evaluate the effect of *pknG* deletion on *M. tuberculosis* proteome using different approaches. Our results clearly show that the global proteome was remodeled in the absence of PknG and shed light on new molecular mechanism underlying PknG role. Altogether, this work contributes to a better understanding of the molecular bases of the adaptation of *M. tuberculosis*, one of the most deadly human pathogens, to its host.

Abbreviations: DIGE, Difference In-Gel Electrophoresis; Dotp, dot products; FDR, false discovery rate; PAT, polyacyltrehaloses; PDIM, phthiocerol dimycocerosate; PRM, Parallel Reaction Monitoring; STD, internal standard; STPK, Ser/Thr protein kinase; TA, toxin-antitoxin; TB, tuberculosis; TCS, two-component system.

* Corresponding author at: Institut Pasteur de Montevideo & Instituto de Investigaciones Biológicas Clemente Estable, Unidad de Bioquímica y Proteómica Analíticas, Mataojo 2020, Montevideo 11400, Uruguay.
E-mail address: duran@pasteur.edu.uy (R. Durán).
[1] Magdalena Gil's current address is Institut Pasteur, Unit of Dynamics of Host-Pathogen Interactions & CNRS UMR3691, Paris, France.
[2] Alessandro Cascioferro's current address is Calibr, a division of The Scripps Research Institut, La Jolla, CA 92037, USA.

https://doi.org/10.1016/j.jprot.2021.104276
Received 26 March 2021; Received in revised form 13 May 2021; Accepted 20 May 2021
Available online 24 May 2021

1. Introduction

Tuberculosis (TB) is a pulmonary disease caused by *Mycobacterium tuberculosis* that remains a major global health problem, being responsible for around 1.4 M deaths worldwide during 2019 [1]. In addition, currently available pharmacological approaches for TB treatment are being challenged by the emergence of drug-resistant, multidrug-resistant, and extensively drug-resistant variants of *M. tuberculosis* [1]. Clinically, TB can be an active (transmissible and symptomatic), subclinical (transmissible but without symptoms), or latent disease (non-transmissible and asymptomatic) [2]. It is estimated that around a quarter of the human population is affected by the latent form of TB, which constitutes a large reservoir for the pathogen [1]. The main pathogenic characteristic of *M. tuberculosis* is its ability to arrest phagosome maturation, allowing bacterial survival and replication inside a relatively harmless vacuole [3]. Macrophage infection triggers a localized pro-inflammatory response that leads to the formation of granulomas, a hallmark of TB, where *M. tuberculosis* can persist for decades in a protected environment, mostly in a dormant state under hypoxic conditions [4]. In the human host, *M. tuberculosis* encounters many different ecological niches and exhibits various physiological states. Thus, it is not surprising that *M. tuberculosis* has developed some very peculiar structural traits and a diversity of regulatory and metabolic capabilities to cope with these different stress conditions.

The impermeable cell envelope is a distinctive characteristic of mycobacteria. It is composed of a central core of peptidoglycan covalently attached to arabinogalactans esterified with mycolic acids, which constitute the inner leaflet of the mycomembrane. Externally, there is an additional layer composed of non-covalently attached (glyco)lipids that are very important for pathogenesis and the host-bacterium interaction [5,6].

Additionally, *M. tuberculosis* has developed a variety of strategies to withstand host's stress conditions: an unusually high number of toxin-antitoxin systems (TA systems) [7], different mechanisms to resist the host oxidative attack [8] and to adapt to low nutrient concentration, as well as low oxygen tension [9,10] and protein phosphorylation systems based on bacterial "eukaryotic-like" Ser/Thr protein kinases (STPKs) and two-component systems (TCS). Concerning the latter, the DosSR two-component system is crucial for the bacterial adaptation to the redox status and to low oxygen concentrations through the induction of around fifty genes comprised within the mycobacterial Dormancy Survival Regulon (DosR regulon, also known as DevR regulon) [11–14].

Among STPKs, PknG was shown to play an important role in bacterial survival within the host, in bacterial metabolism, and in pathogenesis [15–19]. PknG participates in phagosome maturation inhibition promoting *M. tuberculosis* survival inside macrophages [15] and facilitates bacterial growth under *in vitro* stress conditions, such as nutrient deprivation, acid stress, and hypoxia [20,21]. PknG additionally contributes to the intrinsic antibiotic resistance of pathogenic mycobacteria, as the deletion of *pknG* caused a multidrug sensitive phenotype [22]. Moreover, the activity of several enzymes that participate in glutamate metabolism is regulated by PknG through the phosphorylation of the FHA-domain-containing substrate GarA [17]. PknG also phosphorylates the ribosomal protein L13, triggering the regulation of the activity of the Nudix hydrolase RenU [23]. Phosphoproteomics, interactomics and protein array studies have allowed to expand the list of putative mycobacterial PknG substrates [24–26], which currently comprises up to 31 proteins phosphorylated by this kinase either *in vivo* or *in vitro* [27]. However, the physiological relevance of these phosphorylation events and their possible relationship to the proposed roles of the kinase in bacterial survival within the host are not yet fully understood.

The objective of this work was to contribute to the elucidation of the biological processes regulated by PknG in mycobacteria. For this purpose, we employed two complementary quantitative proteomic approaches, 2D-DIGE (Differential In Gel Electrophoresis) and label-free LC-MS/MS, to analyze protein extracts from *M. tuberculosis* H37Rv and a mutant strain lacking PknG. A former DIGE analysis comparing *M. tuberculosis* H37Rv and Δ*pknG* was focused on two proteins that presented pI variations compatible with protein phosphorylation [24]. In the present work, DIGE analysis on the same gels set was performed with a global proteome perspective. LC-MS/MS and DIGE approaches jointly shortlisted around 300 differentially abundant proteins. We show that *M. tuberculosis* H37Rv Δ*pknG* presents altered levels of proteins involved in response to hypoxia, TA systems and synthesis of the core as well as outer layer lipids of the cell wall. Altogether, these results allow us to postulate that the regulation of the expression levels of proteins that are essential for bacterial fitness to host stress conditions is an important mechanism supporting the reported effects of PknG on bacterial survival within the host.

2. Material and methods

2.1. Mycobacterial cultures and protein extract preparation

The *Mycobacterium tuberculosis* pknG null mutant strain (Δ*pknG*) was kindly provided by Josef Av-Gay [18]. Wild-type *M. tuberculosis* H37Rv (WT) and Δ*pknG* strains were cultured in 50 mL of Middlebrook 7H9 medium supplemented with 0.05% Tween® 80, albumin-dextrose and asparagine (BD Biosciences) until early-logarithmic phase as previously described [19]. Mycobacterial cells were washed with PBS buffer, resuspended in minimum medium supplemented with 10 mM asparagine and cultured for five additional days. Cells were harvested by centrifugation (3000 *g* for 10 min at 4 °C), washed in PBS buffer containing the Complete EDTA-free Protease Inhibitor Cocktail (Roche) in the amount recommended by the supplier. To prepare whole cell lysates, an equal amount of acid-washed glass beads (≤106 μm, Sigma) was added to the cell suspension and the system was vortexed at maximum speed for 10 min. Cell debris and beads were removed by centrifugation at 1000 *g* for 5 min at 4 °C and lysates filtered through 0.22 μm PVDF membranes and stored at −80 °C for further analysis. Protein quantification was performed by gel densitometry measurements using the 1D analysis module of the ImageQuant TL software (v8.1) and the LMW-SDS Marker Kit (GE Healthcare) as standard. Protein extracts for the WT and Δ*pknG M. tuberculosis* strains were prepared in triplicate.

2.2. Differential In-Gel Electrophoresis (DIGE)

Differential and quantitative analyses between *M. tuberculosis* strains WT and Δ*pknG* were carried out for three biological replicates employing the Ettan DIGE System (GE Healthcare) following manufacturer's recommendations [28] and as described [24]. Briefly, 100 μg of each protein extract were concentrated using the 2D Clean-up kit (GE Healthcare) and then resuspended in 30 mM Tris pH 8.5, 7 M urea, 2 M thiourea, 4% CHAPS. Twenty-five μg of each WT and Δ*pknG* samples were combined to prepare the internal standard (STD) used for 2D-DIGE image matching, spot volume normalization and abundance change determinations.

Fifty μg of each STD, WT, and Δ*pknG* samples were differentially labeled with cyanine dyes Cy2, Cy3, and Cy5 following the manufacturer's instructions (GE Healthcare) [28]. To compensate for any labeling bias, Cy3 and Cy5 were alternatively employed to label the WT and ΔpknG proteomes, while Cy2 was exclusively used for labeling the STD. Differentially labeled WT, ΔpknG, and STD samples were mixed and the rehydration solution (7 M urea, 2 M thiourea, 4% CHAPS, 0.5% IPG Buffer 4–7 [GE Healthcare]) was added before overnight IPG-strips passive rehydration (pH gradient 4–7, 13 cm).

Isoelectric focusing was performed in an IPGphor Unit (Pharmacia Biotech) employing the previously recommended voltage profile [29]. Then, IPG-strips were treated for 15 min in equilibration buffer (6 M urea, 75 mM Tris–HCl pH 8.8, 29.3% glycerol, 2% SDS, 0.002% bromophenol blue) with the addition of 10 mg/mL DTT and next in the same buffer with 25 mg/mL iodoacetamide. The second-dimension

separation was carried on a 12.5% SDS-PAGE in a SE 600 Ruby Standard Dual Cooled Vertical Unit (GE Healthcare) at 20 °C. Images from gels were obtained employing a Typhoon FLA 9500 variable mode laser scanner (GE Healthcare) at a resolution of 100 μm using the laser wavelength and the filter settings indicated for each dye [30]. The photomultiplier tube voltage was adjusted on each channel to give maximum pixel values below saturation levels (60,000–90,000 counts).

The analysis of images was performed using DeCyder™ 2D software (v7.2) (GE Healthcare). The DeCyder's Differential In-gel Analysis module (DIA) was employed for spots co-detection, quantification by normalization, and ratio calculation. The DeCyder's Biological Variation Analysis module (BVA) was utilized for gel-to-gel spot matching and statistical analysis, allowing quantitative comparisons of spot volumes across multiple gels. An unpaired Student's *t*-test was used to assess significant changes. Spots displaying significant differences (p-value ≤ 0.05) and a fold-change greater than 25% were selected for further analyses.

2.3. Protein identification by MALDI-TOF/TOF MS

Differential spots were matched to the silver-stained master gel and were picked and processed for MALDI-TOF/TOF analysis following previously reported protocols [31,32].

Mass spectra of peptides mixtures were acquired in a 4800 MALDI TOF/TOF instrument (ABiSciex, USA) in positive ion reflector mode. Mass spectra were calibrated using a mixture of peptides standard (Applied Biosystems) and trypsin autolysis products. Some peptides from all protein spots were selected for MS/MS analyses using the following settings: 8 kV and 15 kV for sources 1 and 2, respectively.

Protein identification was performed by database searching of acquired m/z values employing the MASCOT search engine (Matrix Science http://www.matrixscience.com/search_form_select.html) in the Sequence Query mode, using a database from NCBI (20170811), and applying the following search parameters: monoisotopic mass tolerance, 0.05 Da; fragment mass tolerance, 0.5 Da; Met oxidation and Ser/Thr/Tyr phosphorylation as variable modifications, Cys carbamidomethylation as fixed modification, and allowance of one missed tryptic cleavage. Protein mass was unrestricted and taxonomy was limited to *Mycobacterium tuberculosis* complex. Significant protein scores (p-value < 0.05) were used as criteria for confident identification.

2.4. nanoLC-MS/MS analysis and protein identification

Total protein extracts (20 μg) from WT and Δ*pknG* samples (in triplicates) were reduced with 10 mM DTT at 56 °C for 60 min and then alkylated with 55 mM iodoacetamide at room temperature for 45 min and in the darkness. The samples were separated by SDS-PAGE using precast 4%–12% gradient gels (NuPAGE, MES System, Invitrogen) and stained with colloidal Coomassie Brilliant Blue G-250. Each lane was excised into ten slices that were destained by incubation with 0.2 M ammonium bicarbonate/ACN (1:1) for 1 h at room temperature with agitation. *In-gel* proteolytic digestion and peptide extraction were performed as described earlier [24]. Peptide samples were vacuum dried, resuspended in 0.1% formic acid and injected into a nano-HPLC system (EASY-nLC 1000, Thermo Scientific) equipped with a reverse-phase column (EASY-Spray column, 50 cm × 75 μm ID, PepMap RSLC C18, 2 μm, Thermo Scientific). Peptides separation was performed at a constant flow rate of 250 nL/min and using a gradient from 0% to 50% of mobile phase B (mobile phase A: 0.1% formic acid, mobile phase B: 0.1% formic acid in acetonitrile) over 100 min. Peptide analysis was performed in an LTQ Velos nano-ESI linear ion trap equipment (Thermo Scientific) in a data-dependent acquisition mode. Xcalibur 2.1 was used for data acquisition in two steps: 1. acquisition of full MS scan in the positive ion mode with m/z between 300 and 1800 Da, 2. sequential fragmentation of the ten most intense ions with a normalized collision energy of 35, an isolation width of 2 m/z. The activation Q was set on 0.25, the activation time on 15 ms, and a dynamic exclusion time of 30 s. MS source parameters were set as follows: 2.3 kV electrospray voltage and 260 °C capillary temperature.

PatternLab for Proteomics (version 4.0.0.74) [33] was employed to generate a target-decoy database using sequences from *M. tuberculosis* H37Rv (taxon identifier: 83332; 3993 sequences) downloaded from the UniProt consortium in October 2017. In addition, 127 common mass spectrometry contaminants were included [33] giving rise to a target-reverse database with 8228 entries.

The Comet search engine was operated using the following parameters: trypsin as proteolytic enzyme with full specificity; oxidation of Met and phosphorylation on Ser/Thr/Tyr as variable modifications, carbamidomethylation of Cys as fixed modification; and 800 ppm of tolerance from the measured precursor m/z. XCorr and Z-Score were used as the primary and secondary search engine scores, respectively.

Peptide spectrum matches were filtered using the Search Engine Processor (SEPro) and acceptable false discovery rate (FDR) criteria were set on ≤1% at the protein level, and ≤2% at the peptide level. The actual FDR for each file searched is depicted in Supplementary Table S1. PatternLab's statistical model for the Approximately Area Proportional Venn Diagram module was used to compare conditions and determine proteins that are likely to be exclusively detected in each situation due to differences in its abundance (p-*value* < 0.05). The Bayesian model integrated into PatternLab for Proteomics [34] considers quantitative data and the number of appearances in different biological replicates to assign p-values. PatternLab's T-Fold module was used to detect proteins present in both conditions at significantly different levels by spectral count analysis. Buzios and Clustergram modules were used to perform a Principal Component Analysis and a Heatmap, respectively [33].

2.5. Parallel Reaction Monitoring (PRM) targeted MS

Some proteins, found to display differential abundances by discovery proteomics, belonging to the metabolism of the outermost lipids of the mycobacterial cell envelope (Mas and Msl3) or involved in the response to hypoxia (Icl, Ald, Lat, Rv2030c, Acg, DevR, hspX, Hrp-1) were chosen to be validated by tier 3 targeted proteomic analysis.

For Parallel Reaction Monitoring (PRM) analysis, 20 μg of WT and Δ*pknG* samples were run 1 cm on a resolving SDS-PAGE and processed for mass spectrometry analysis as described above, using 20 μL of mobile phase A to resuspend them.

To generate the spectral library, 5 μL of each sample were mixed and separated using a nano-HPLC (UltiMate 3000, Thermo) coupled to a Q-Orbitrap mass spectrometer (Q Exactive Plus, Thermo). Tryptic peptides (5 μg) were injected into an Acclaim PepMap™ 100 C18 nano-trap column (75 μm × 2 cm, 3 μm particle size, Thermo) and separated in a 75 μm × 50 cm, PepMap™ RSLC C18 analytical column (2 μm particle size, 100 Å, Thermo) at a constant flow rate of 200 nL/min and 40 °C. The column was equilibrated with 1% of mobile phase B, and the elution was performed using a gradient from 1% to 50% of mobile phase B over 180 min and 50% to 99% over 15 min. The ion spray voltage setting was 1.7 kV, the capillary temperature was set at 250 °C and S-lens RF level at 50. Mass analysis was performed in a data-dependent mode in two steps: 1. acquisition of full MS scan in a 200 to 2000 m/z range; 2. fragmentation of the 12 most intense ions in each segment by HCD using a stepped normalized collision energy of 25, 30, and 35. The following settings were used for full MS scans: a resolution of 70,000 at 200 m/z, an AGC target value of 1E06, and a maximum ion injection time of 100 ms. For MS/MS acquisition the resolution was 17,500 at 200 m/z, AGC target value of 1E05, and maximum injection time of 50 ms. Precursor ions with unassigned, single, and higher than five charges were excluded. The dynamic exclusion time was set at 10 s. Two technical replicates of the sample mix were used to generate the library. Thermo raw files were searched against the target-decoy *M. tuberculosis* H37Rv database as described above but using PatternLab (v5). Search was performed with 40 ppm for precursor mass accuracy and results were

afterwards filtered using 5 ppm error tolerance. The result file was saved in SSL format as .raw file (Thermo), with carbamidomethylation of Cys as a fixed modification, to interface with Skyline software.

Taking into account the *M. tuberculosis* H37Rv background proteome downloaded from the UniProt server (www.uniprot.org) and the generated spectral library data, 23 peptides derived from the 11 chosen proteins were selected using Skyline (v. 20.1.0.155). Since in some cases a unique theoretical quantotypic peptide match confidently with those of *M. tuberculosis* spectral library, some proteins were validated with just one peptide. An unscheduled isolation list was generated, loaded into Thermo Xcalibur 4.0.27.19 and used to carry out a PRM analysis on the Q Exactive Plus mass spectrometer. Five μg of WT and Δ*pknG* samples were injected in duplicates and peptides were separated using the same gradient used for spectral library generation. The mass spectrometer settings were as follows: positive polarity, a resolution of 17,500 at 200 *m/z*, AGC target value of 2E04, maximum injection time of 50 ms, 2.0 *m/z* of isolation window, stepped normalized collision energy of 25, 30, and 35.

The list of the targeted peptides in the PRM analysis is shown in Supplementary Table S2.

Resulting PRM raw data was extracted and imported into Skyline software (v20.2) for analysis. Data were manually refined using the spectral library as a reference, taking into account the dotp values for each peptide, and the comparison of peak areas for each transition.

For quantitative comparative analyses between WT and Δ*pknG* peptides, the sum of the peak areas of the transitions of each peptide and the equalization to medians were employed. Peptides with a significant difference showing an adjusted p-value < 0.05 were considered.

2.6. Bioinformatics analyses

The functional classification of identified proteins was performed using the information provided by the Mycobrowser server (https://mycobrowser.epfl.ch/).

A statistical overrepresentation test was performed using the Panther Server Classification System (http://pantherdb.org) version 15.0, released 2020-02-14 [35]. The annotation data set "GO biological processes complete" (released 2020-07-28) was used. The release date of the GO ontology dataset was 2020-10-09. Protein showing significant abundance changes, by both 2D-DIGE and label-free LC-MS/MS approaches, were used for the analysis. Proteins that only show changes in proteoforms patterns were excluded. The *M. tuberculosis* database was used as a reference list.

2.7. Data availability

The mass spectrometry proteomic raw data have been deposited to the ProteomeXchange Consortium *via* the PRIDE partner repository with the dataset identifier PXD023975 for discovery proteomics data and PXD023956 for targeted proteomics data [36].

3. Results

To identify proteins and processes altered in a *M. tuberculosis pknG* deletion mutant that could be responsible for the previously observed phenotypes in bacterial survival, we compared the proteomes of wild-type *M. tuberculosis* H37Rv (WT) and Δ*pknG* using two complementary quantitative approaches: 2D-DIGE and label free LC-MS/MS analysis.

3.1. 2D-DIGE analysis revealed that proteins involved in lipid metabolism and stress adaptation are altered in M. tuberculosis ΔpknG

Protein extracts from *M. tuberculosis* WT and Δ*pknG* cells were prepared in triplicates and analyzed by 2D-DIGE [24]. A representative 2D-DIGE gel image, showing WT proteins labeled with Cy5 dye (red spots) and Δ*pknG* proteins labeled with Cy3 (green spots), is depicted in Fig. 1.

Image analysis allowed detecting 111 spots with statistically significant abundance differences between the two strains (fold-changes >25%; p-value ≤ 0.05), 30 of which were overrepresented while 81 were underrepresented in Δ*pknG*. Sixty-six spots could be confidently excised from the post-stained master gel and MALDI TOT/TOF MS analysis led to the identification of 27 different proteins from 36 spots (Supplementary Fig. S1). More than one protein was identified in two spots (spots 27 and 36), and therefore they were not considered for further analyses. Several differential spots were previously assigned to proteoforms of GarA and GlnA1 [24], two earlier reported substrates of PknG involved in nitrogen metabolism [17,19,24]. Thirty-six new differential spots, indicated in Fig. 1, emerged from this analysis (further details are given in Supplementary Table S3). Many of the underrepresented proteins in Δ*pknG* are involved in lipid metabolism processes, including fatty acid degradation (FadA, EchA16 and FadA4), biosynthesis of unsaturated fatty acids (DesA2), biosynthesis of mycolic acids (KasA) and triacylglycerol metabolism (FbpB). Notably, 10 underrepresented spots in the Δ*pknG* strain corresponded to proteins upregulated in hypoxic and other growth-limiting conditions that usually lead to non-replicative mycobacteria [4,37–41]. These spots corresponded to the bacterioferritin BrfB, the heat shock protein HspX, isocitrate lyase Icl, the elongation factor Tu and the secreted L-alanine dehydrogenase Ald (Fig. 1 and Supplementary Table S3). Conversely, the uncharacterized proteins Rv2557 and Rv2558, which were previously reported to be overexpressed in *M. tuberculosis* under starvation conditions [42], were found to be overrepresented in the Δ*pknG* strain. Some of the identified proteins led to more than one spot, and some of them had not the expected pI and/or MW, possibly reflecting the presence of post-translational modifications or proteolysis.

Overall, our 2D-DIGE analysis suggested that *M. tuberculosis* Δ*pknG* presents alterations in glutamate as well as lipid metabolism and has modified levels of proteins (and/or its proteoforms) required for the bacterial adaptation to stress conditions known to induce a persistent

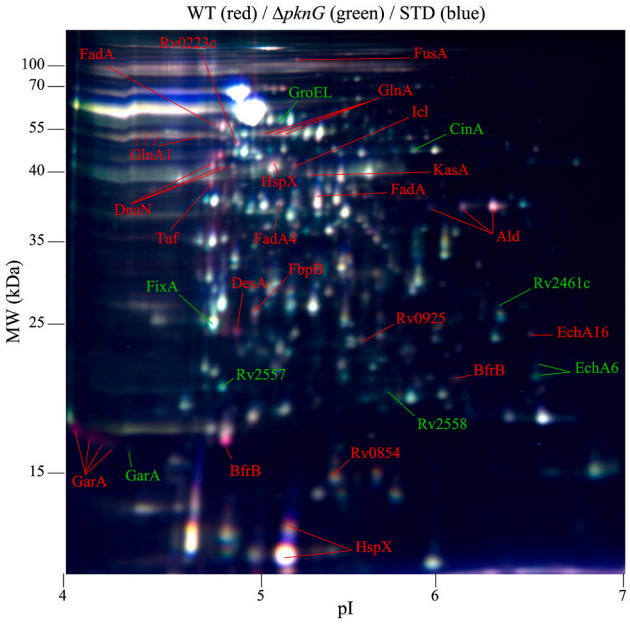

Fig. 1. Representative 2D-DIGE image of total protein extracts from *M. tuberculosis* H37Rv WT and Δ*pknG* strains. Overlay image of WT (labeled with Cy5, red), Δ*pknG* (labeled with Cy3, green), and the internal standard (STD, labeled with Cy2, blue). Identified differential spots (considering all replicates, p-value ≤ 0.05 and fold-changes $\geq$25%) are shown. Red and green labels indicate spots overrepresented in WT and Δ*pknG*, respectively. GarA and GlnA1 spots were previously identified [24]. Details regarding 2D-DIGE analyses and protein identification values for all the other differential spots are depicted in Supplementary Fig. 1 and Supplementary Table S3.

state.

3.2. Label-free LC-MS/MS analysis indicated that the cell envelope lipid biosynthesis, hypoxia, and other stress-related processes are altered in *M. tuberculosis* Δ*pknG*

LC-MS/MS analysis allowed identifying an average of 1513 proteins among replicates, which correspond to approximately 38% of the total proteins encoded by *M. tuberculosis* H37Rv, denoting a substantial coverage of the proteome. Supplementary Table S1 shows all proteins detected in each replicate, its UniProt accession number, number of unique peptides, sequence counts, spectrum counts, normalized spectral abundance factor (NSAF), protein sequence coverage as well as protein score. Information concerning peptides assigned to each protein (including precursor charge at maximum primary score and observed peptide modifications) is provided in Supplementary Table S4.

Using the Venn diagram's statistic module from the PatternLab for Proteomics software [33] 1854 proteins were identified in both conditions, 59 proteins were exclusively detected in *M. tuberculosis* WT and 32 proteins were solely detected in Δ*pknG* (p-value < 0.05) (Supplementary Table S5). Then, we used the statistics PatternLab for Proteomics TFold module to compare the proteins present in both proteomes but with differential abundance [33]. Considering proteins present in at least 4 of the 6 biological replicates used in this study, 137 proteins were found with statistically different levels in Δ*pknG* samples when compared to WT (q-value < 0.05) (Fig. 2 and Supplementary Table S5), 45 of them were overrepresented while 92 were underrepresented in *M tuberculosis* Δ*pknG*.

A principal component analysis (PCA) performed on the samples using the Búzios module of Patternlab for Proteomics showed the correct grouping of the WT and Δ*pknG* sample sets, confirming the consistency in the global observed proteomic changes (Supplementary Fig. S2). In addition, hierarchical clustering classified the three replicates of the WT strain in the same hierarchical cluster but different form the one of the Δ*pknG* replicates (Supplementary Fig. S3).

As expected, among the proteins exclusively detected in WT, PknG was the one identified with the highest number of spectra, followed by PhoH2, a protein comprising a TA system with RNAse activity [43]. Additional TA system members were also detected exclusively in WT proteomes (the toxins VapC38, VapC37, HigB2; and the antitoxins VapB24 and MazE3).

Notably, many proteins that integrate the DosR regulon showed decreased abundance in Δ*pknG*. Three of them (the 6-phosphofructokinase PfkB, the conserved hypothetical proteins Rv2003c and Rv3134c) were uniquely detected in the WT dataset and many others were underrepresented in Δ*pknG,* including vitamin B12-dependent ribonucleoside-diphosphate reductase NrdZ, Rv2004c, Rv2030c, the putative NAD(*P*)H nitroreductase Acg, the hypoxic response protein Hrp-1, Rv2629, Rv3127, the probable diacylglycerol O-acyltransferase Tgs, Rv3131 and the response regulator DosR itself (Fig. 2, Table 1, Supplementary Table S5) [12,14,44]. In a similar vein, other proteins important for the hypoxia-induced persistent state [40,41,45,46] were diminished in Δ*pknG*, such as the isocitrate lyase Icl, the secreted L-alanine dehydrogenase Ald, and the probable L-lysine-epsilon aminotransferase Lat (Fig. 2, Supplementary Table S5). In addition, a set of proteins involved in redox sensing and reaction to host oxidative attack also showed decreased abundance in Δ*pknG*, including IdeR (an iron-dependent response regulator that also senses redox status) [47]; the bacterioferritin BfrB [48], the thioredoxin reductase TrxB and DosR, which responds to changes in both oxygen tension and redox status [10].

Remarkably, the proteins that showed the highest fold-changes among the differential protein dataset are enzymes involved in the synthesis of non-covalently attached outer layer lipids of the complex mycobacterial cell envelope (Table 2). The probable multifunctional mycocerosic acid synthase membrane-associated protein Mas was overrepresented in the WT strain (fold-change 19.9) while the mycolipanoate synthase Msl3 was overrepresented in the Δ*pknG* strain (fold-change 9.3). Besides, the protein *N*-acetylglucosamine-6-phosphate deacetylase NagA, involved in *N*-acetyl glucosamine utilization, is

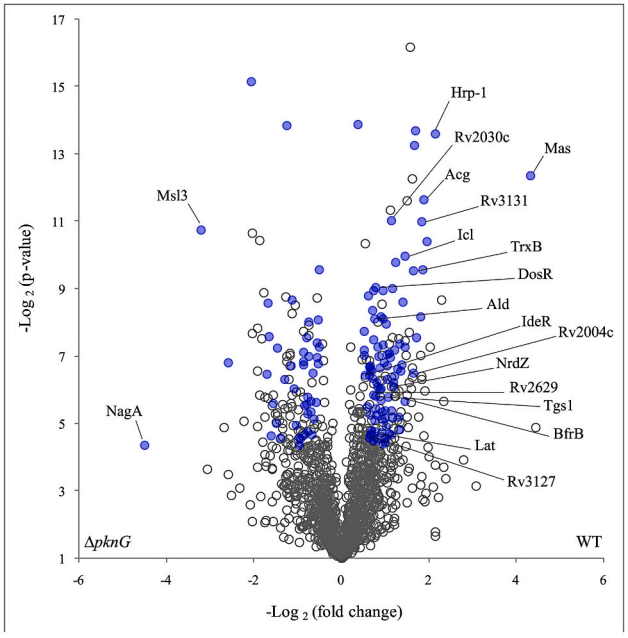

Fig. 2. Differentially abundant proteins between *M. tuberculosis* H37Rv WT and Δ*pknG*. PatternLab's TFold module was used to pinpoint proteins found in both conditions but showing a statistically differential abundance (BH q-value <0.05). The volcano plot shows the Log_2 (p-value) on the y-axis and the Log_2 (fold-change) on the x-axis. Proteins present in at least 4 of the 6 total replicates used for the analysis (3 Δ*pknG* replicates and 3 WT replicates) are represented by a dot in the plot. Blue dots correspond to proteins satisfying all statistical filters and thus are considered as differentially abundant proteins between strains. Selected differential proteins discussed in the text are labeled and all the information regarding differential proteins is depicted in Supplementary Table S5.

Table 1
Proteins of DosR regulon statistically underrepresented in Δ*pknG*.

Proteins exclusively detected in WT (p-value < 0.05)				
Protein	Tuberculist ID	Description		
Rv2003c	Rv2003c	Uncharacterized protein		
PfkB	Rv2029c	Putative ATP-dependent 6-phosphofructokinase isozyme 2		
Rv3134c	Rv3134c	Universal stress protein		
Proteins detected in both conditions, underrepresented in Δ*pknG*				
Protein	Tuberculist ID	Fold-change	p-value	Description
Hrp-1	Rv2626c	4.4	0.0001	Hypoxic response protein 1
Rv2030c	Rv2030c	2.2	0.0005	Uncharacterized protein
Acg	Rv2032	3.7	0.0003	Putative NAD(*P*)H nitroreductase
DosR	Rv3133c	1.7	0.0019	Transcriptional regulatory protein DosR
Rv3131	Rv3131	2.83	0.0069	Putative NAD(*P*)H nitroreductase
Tgs1	Rv3130c	1.7	0.0171	Probable diacylglycerol O-acyltransferase
Rv2004c	Rv2004c	2.8	0.0198	Uncharacterized Protein
NrdZ	Rv0570	2.2	0.0248	Vitamin B12-dependent ribonucleoside-diphosphate reductase
Rv2629	Rv2629	1.7	0.0260	Uncharacterized protein
Rv3127	Rv3127	1.6	0.0354	Uncharacterized protein

the protein that exhibited the highest fold-change among those over-represented in the Δ*pknG* dataset (fold-change 22.5) [6]. Also, many proteins that participate in mycolic acids biosynthesis were underrepresented in Δ*pknG* proteome, among them KasA, MmaA1, MmaA3, MmaA4, CmaA1, CmaA2, FbpB (Table 2 and Supplementary Table S5). In summary, our label-free LC-MS/MS analysis revealed that *pknG* deletion affects the relative abundance of enzymes involved in the biogenesis of the mycobacterial cell envelope, proteins involved in stress response mediated by TA systems and redox homeostasis. Moreover, PknG seems to directly or indirectly regulate the levels of expression of proteins that play essential roles in adapting *M. tuberculosis* to hypoxic conditions.

Supporting this, functional enrichment analysis using differential proteins identified by 2D-DIGE and shotgun approaches indicated that the main biological process altered in *M. tuberculosis* Δ*pknG* is response to hypoxia (Supplementary Table S6). Also, consistent with the differential proteins discussed above, the biological processes "fatty acid biosynthetic process" and "oxidation-reduction" were statistically enriched in the WT proteome (Supplementary Table S6).

3.3. Validation of differentially abundant proteins by Parallel Reaction Monitoring (PRM)

To further confirm the relative abundance of some selected proteins we used a targeted proteomic strategy (PRM). After the refinement of peptide chromatograms using Skyline, we focused on two proteins that participate in the biosynthesis of lipids of the outermost layer of the cell envelope (Mas and Msl3) and 7 proteins involved in the response to hypoxia (Ald, Acg, DevR, Hrp-1, Icl, Lat, Rv2030c). We successfully validated the changes in the relative abundance of 5 of the 9 analyzed proteins (adjusted p-value < 0.05), namely Msl3, Mas, Hrp-1, Rv2030c, and Acg (Figs. 3 and 4). The quite large fold-changes recorded in the Δ*pknG* strain for Msl3 (2995-fold increment) and Mas (100-fold decrease) denoted a clear switch in enzymes responsible for the synthesis of free lipids in the outer layer of *M. tuberculosis* cell envelope. Among the proteins involved in response to hypoxia, Hrp-1 showed the highest expression reduction in the Δ*pknG* mutant (12.5 times) (Figs. 3 and 4). Thus, our results allow confirming that *pknG* deletion impacts on the outer lipids biosynthesis and the response to low-oxygen levels, two relevant physiological processes for the host-pathogen interaction and the bacterial survival within infected human cells.

4. Discussion

In a previous work we performed a 2D-DIGE analysis of WT and Δ*pknG M. tuberculosis* to identify substrates of PknG [24]. Besides the differences in phosphorylation patterns, this analysis suggested that the strain lacking *pknG* had a more global proteomic change. In this work, we employed two comparative and quantitative proteomic approaches to assess the effect of *pknG* deletion on the total proteome of *M. tuberculosis*. Comprehensive proteomic profiling of *M. tuberculosis* Δ*pknG* indicated that as much as 15% of the detected proteins presented

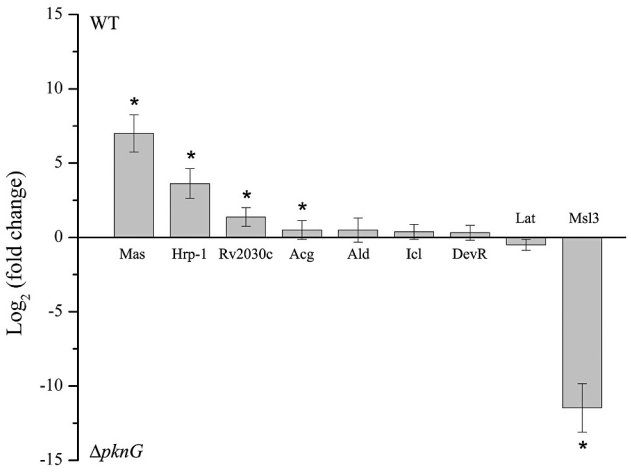

Fig. 3. Validation of protein relative abundance changes by targeted proteomics (PRM). Bar graph showing the Log_2(fold-change) of the proteins analyzed by PRM. The sum of transition areas was used as a quantitative measure and equalization to medians was employed for normalization. Positive values represent proteins increased in WT *M. tuberculosis* and negative values in the Δ*pknG* strain. Proteins showing statistically significant changes are indicated with an asterisk (adjusted p-value ˂ 0.05).

significant abundance changes compared to WT (5.7% of the predicted *M. tuberculosis* H37Rv proteins), pointing to a substantial remodeling of the proteome in the absence of PknG. Proteins with altered expression levels consistently mapped into defined biological processes relevant for virulence and bacterial survival within infected human cells.

During more than ten years, various research groups have contributed to an extensive phenotypic and functional characterization of mycobacteria lacking PknG, and the accumulated evidence clearly indicates that this kinase is crucial for pathogenicity. It was shown early that *M.tuberculosis* Δ*pknG* caused delayed mortality of highly susceptible infected mice, and presented decreased viability in an immunocompetent mice model [18]. Furthermore, deletion of *pknG* has shown to impair granuloma formation in guinea pigs [20] and more recently a decreased capability of Δ*pknG* to resuscitate in a latent tuberculosis mouse model was reported [49]. It was also demonstrated that the absence of PknG prevents mycobacterial survival within host macrophages [15] and leads to a growth defect under *in vitro* models of hypoxia [20]. Finally, several pieces of evidence point to an altered cell envelope in the absence of PknG. Wolff et al. reported that a *Mycobacterium smegmatis* Δ*pknG* mutant strain presented severely altered cell surface properties, in terms of charge and hydrophobicity, and also showed that PknG is required for biofilm formation in several mycobacterial species, including *M. tuberculosis* and *Mycobacterium bovis* BCG [23]. In addition, a diminished intrinsic resistance to antibiotics, possibly mediated by an altered permeability and hydrophobicity of bacterial cells, was reported for *M. smegmatis* Δ*pknG* [22].

Despite the overwhelming evidence supporting a role of PknG in

Table 2
Proteins involved in cell envelope metabolism showing statistically differential abundance between strains.

Protein	Tuberculist ID	Fold-change	p-value	Increased in:	Description
Mas	Rv2940	19.9	0.0002	WT	Probable multifunctional mycocerosic acid synthase membrane-associated Mas
Msl3	Rv1180/Rv1181	9.3	0.0006	Δ*pknG*	Mycolipanoate synthase
NagA	Rv3332	22.5	0.0489	Δ*pknG*	*N*-acetylglucosamine-6-phosphate deacetylase
MmaA3	Rv0643c	2.7	0.0066	WT	Methoxy mycolic acid synthase
CmaA2	Rv0503c	2.1	0.0093	WT	Cyclopropane mycolic acid synthase 2
MmaA4	Rv0642c	1.6	0.0110	WT	Hydroxymycolate synthase
FbpB	Rv1886c	1.8	0.0132	WT	Diacylglycerolacyltransferase/mycolyltransferase Ag85B
CmaA1	Rv3392c	1.7	0.0176	WT	Cyclopropane mycolicacid synthase 1
MmaA1	Rv0645c	1.5	0.0233	WT	Mycolic acid methyltransferase MmaA1
KasA	Rv2245	1.6	0.0264	WT	3-oxoacyl-[acyl-carrier-protein] synthase 1

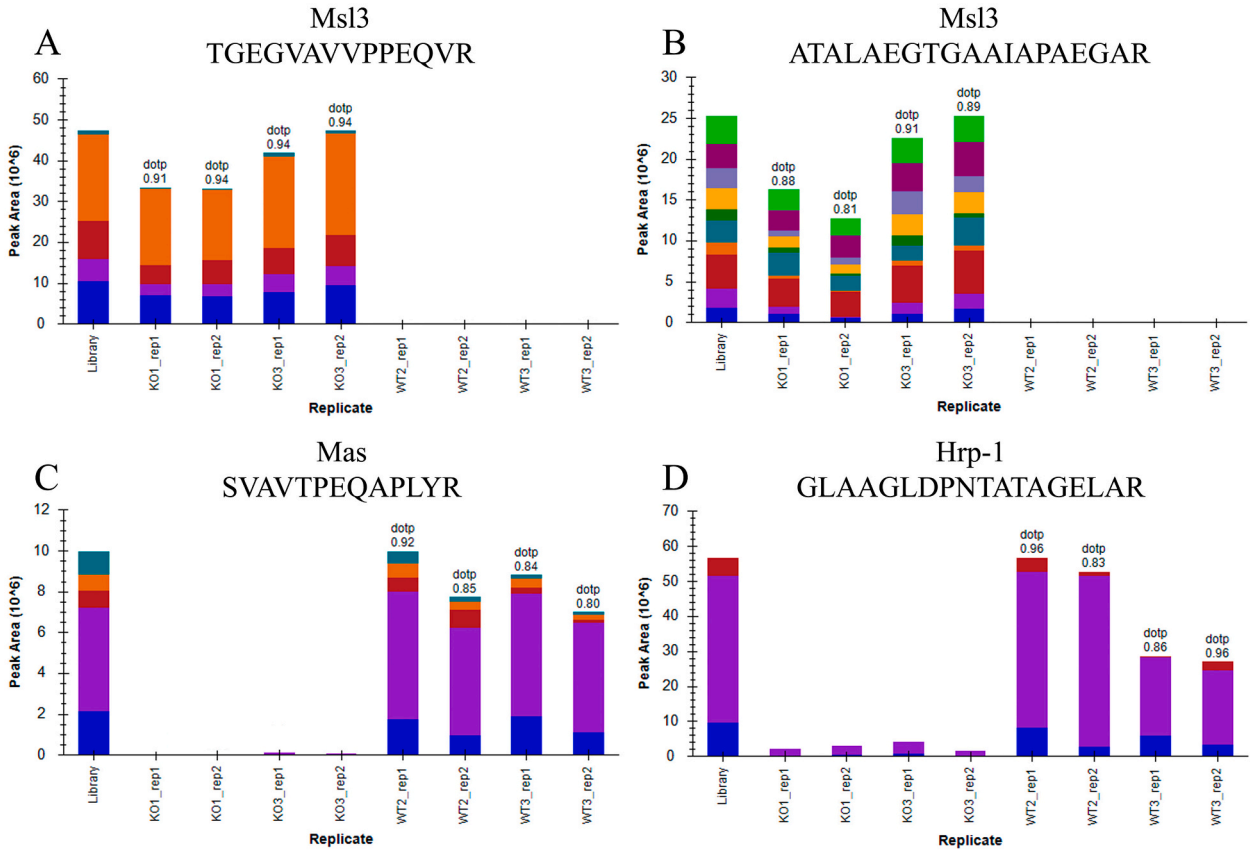

Fig. 4. Changes in the relative abundance of selected peptides determined by PRM. Each bar graph shows the variation in abundance (represented as the sum of transition areas, each color in a bar represents an individual transition area). The dotp value is indicated. The sum of the transition area of each peptide in the library is also shown. Panel A and B: TGEGVAVVPPEQVR and ATALAEGTGAAIAPAEGAR peptides from Msl3 protein. Panel C: SVAVTEQAPLYR peptide from Mas protein. Panel D: GLAAGLDPNTATAGELAR peptide from Hrp-1 protein.

growth inside the host and pathogenicity, the mechanism of action of this kinase at the molecular level is still a subject of extensive debate. While some studies showed that PknG regulation of glutamate and/or redox metabolism could play a key role for bacterial adaptation to the nutrient conditions found inside the host [19,20,23], others proposed that the phosphorylation of host's proteins is a key factor in PknG's mediated virulence [15,50]. The proteomic changes reported here for Δ*pknG* are very consistent with the previously reported phenotypes, and shed some light on new molecular mechanism behind them.

Twenty-seven proteins were identified from 36 differential spots according to 2D-DIGE analysis; while the label-free LC-MS/MS approach allowed the detection of 228 additional differential proteins.

Seven differential proteins involved in response to hypoxia and lipid metabolism were detected using both approaches, with protein abundances changing in the same direction (Ald, BfrB, DesA2, FbpB, Icl, KasA, Rv0223c). Nineteen out of the 20 remaining differential proteins identified by DIGE were also detected in label-free LC-MS/MS experiments, but the differential levels could not be confirmed, either because proteins were identified with few spectra or because changes were not statistically significant. A possible explanation for this observation is that specific proteoforms, in particular phosphorylated ones, were responsible for the 2D-DIGE differential spots.

Very interestingly, the quite large proteomic changes associated with the deletion of this protein kinase mainly involves two relevant processes: cell envelope biogenesis and hypoxia response. These findings are discussed in detail below.

4.1. Cell envelope biosynthesis

Our results indicated that the expression levels of proteins implicated in the biosynthesis of different components of the *M. tuberculosis* cell envelope were altered in Δ*pknG*. Proteins involved in peptidoglycan component recycling and cell wall synthesis were overrepresented in Δ*pknG*. NagA, an enzyme that catalyzes a critical step for the synthesis of peptidoglycan precursors and its recycling [51] was 22.5 fold enriched in Δ*pknG* (Table 2). In addition, several proteins located in an operon related to peptidoglycan synthesis, cell growth and shape (the STPKs PknA and PknB, and the protein FhaA) [52,53], were also overrepresented in the Δ*pknG* dataset (Supplementary Table S5). On the contrary, the biosynthetic pathway of other distinctive components of the cell envelope of these bacteria, mycolic acids, is underrepresented in Δ*pknG* (Table 2 and Supplementary Table S5). Altogether, these observations suggest that PknG could be involved in the regulation of the structure of cell wall core of *M. tuberculosis*.

However, the most important proteomic changes are related to the biosynthetic pathways of other lipid components of the cell envelope. Our results strongly suggest a major change in the composition of the bioactive complex lipids found in the outermost layer of the cell envelope. Two enzymes of the polyketide synthase family that participates in the biosynthesis of branched fatty acids, the Multifunctional mycocerosic acid synthase membrane-associated Mas and the Mycolipanoate synthase Msl3, presented high fold-changes in Δ*pknG*. These impressive fold-changes in opposite directions were further confirmed by PRM targeted proteomics, showing a 100 fold decrease of Mas levels and 2995 fold increase in Msl3 levels in Δ*pknG*. Mas and Msl3 share the same

enzymatic activity and have substantial sequence identity, but participate in different biosynthetic pathways [54]. Mas is involved in the biosynthesis of the cell envelope's phthiocerol dimycocerosates (PDIMs), which are unique for slow growing mycobacteria and have a key role in *M. tuberculosis* pathogenesis [5,54–56]. On the other hand, Msl3 is a Mas-like enzyme involved in the biosynthesis of critical constituents of polyacyltrehaloses (PATs), another kind of free lipids of the cell envelope of *M. tuberculosis* that are also found exclusively in virulent strains [54,57]. However, in contrast to PDIMs, there is experimental evidence showing that PATs are not essential for virulence [54,57]. The Mas enzyme is required for full virulence of *M. tuberculosis* and it was shown to participate in lipid synthesis during infection [58,59]. The products of the biosynthetic pathway in which Mas participates, PDIMs, are one of the very early reported virulence factors of *M. tuberculosis* [60] and have an important role in the fate of the bacteria inside infected cells. Indeed, disruption of genes involved in PDIMs biosynthesis led to strains unable to inhibit phagosome acidification and maturation [61], a phenotype already described for Δ*pknG* [15]. Although the mechanisms underlying PDIMs–mediated virulence are still not fully understood, a role in the modulation of the immune response, the properties of cell surface and the protection against nitrogen reactive species has been reported for this cell envelope component [62,63]. A multidrug-sensitive phenotype for *M. smegmatis* ΔpknG has already been reported [22]. In light of the present results, it would be important to evaluate whether the intrinsic resistance of mycobacteria to several antibiotics is also altered in H37Rv Δ*pknG*. This would be a relevant piece of information to reinforce PknG as a drug target.

Altogether, these observations allow us to postulate that there is a switch in the type of free lipids synthesized by Δ*pknG* in *M. tuberculosis*, with increased levels of PATs and decreased levels of the PDIMs virulence factors. In this scenario, it is tempting to speculate that the much lower levels of Mas, and possibly of its biosynthetic products PDIMs, could contribute to the observed altered physicochemical properties of the cell envelope and the growth defects inside host macrophages previously reported for Δ*pknG*.

4.2. Response to hypoxia

The evidence arising from both, label free LC-MS/MS and DIGE experiments, consistently indicated that proteins involved in the response to hypoxia were downregulated in Δ*pknG*. On one hand, around one third of the underrepresented protein spots in DIGE gels of Δ*pknG* are increased in hypoxia models of *M. tuberculosis* [37,64] (Supplementary Table S3). Shotgun analysis further supported these results revealing that response to hypoxia is the main biological process altered in Δ*pknG*. Adaptation to low oxygen conditions in mycobacteria is mainly mediated by the DosR regulon, which comprises around 50 genes that are upregulated by the DosR response regulator under oxygen limitation conditions [12,65,66]. Our proteomic results allowed us to detect several proteins of this regulon as underrepresented in Δ*pknG* (Table 1). In addition to DosR regulon proteins, several proteins known to be relevant for the entry in the hypoxic non-replicative state were also underrepresented in Δ*pknG*: Ald, Icl, BfrB, Tuf, Lat. All of these differential proteins are thought to be involved in the adaptation of the bacteria to hypoxic conditions and other stress conditions found inside macrophages and granulomas, and are jointly considered a distinctive proteomic hallmark of the mycobacterial response to hypoxia [38–41,65]. Only one of the proteins of this hypoxic proteomic fingerprint could not be detected with altered levels in Δ*pknG*: the HspX protein. HspX and Hrp-1constitute the most paradigmatic DosR regulon induction markers and in turn are the proteins whose levels change most dramatically in response to hypoxia [67,68]. Interestingly enough, while Hrp-1 levels were very significantly decreased in Δ*pknG*, HspX is among the proteins whose global levels were not altered in shotgun analysis, but presented differential spots in 2D-DIGE. This intriguing finding deserves further investigation. One possibility is that PknG, through phosphorylation of specific substrates, may add an additional level of control on the DosR regulon, allowing to differentially tune the levels of its various components. In fact, the regulation of DosR activity by Ser/Thr protein kinases (in addition to the well-studied phosphorylation by His protein kinases) has already been shown. On one hand, phosphorylation of Thr198 and Thr205 by PknH contributes to the DosR dimerization and enhances its transcriptional activity [69]. On the other hand, phosphorylation of DosR Thr180 by overexpression of the catalytic domain of PknB in *M. smegmatis* negatively affected the DNA-binding affinity of the regulator to its target DNA sequence [70]. Thus, an attractive hypothesis is that a defect in DosR phosphorylation in Δ*pknG* could be mediating the low levels of hypoxic response proteins. In fact, published data support this hypothesis. Bae et al. evaluated the interaction between DosR and the 11 STPKs codified by *M. tuberculosis* using yeast two-hybrid assay, and PknG showed the strongest interaction [70]. However, these authors use HspX as a reporter for DosR induction, and this led them to dismiss the possible physiological relevance of the PknG-DosR interaction. Based on our results, HspX is not a good marker of a possible PknG-mediated induction of hypoxia response and the direct phosphorylation of DosR by PknG deserves to be investigated. Indeed, comparative phosphoproteomic analysis of these strains would be a crucial next step in identifying direct substrates of PknG in *M. tuberculosis*, as well as downstream phosphorylated proteins in PknG-mediated signaling pathways.

Altogether, 19 out of 59 proteins exclusively detected in WT, and 38 out of 92 proteins overrepresented in this same strain, have previously been reported to be up-regulated in the proteome of hypoxic bacteria [4,14,38,41,65,69,71,72]. This is in very good agreement with reports showing that mycobacteria lacking PknG were unable to grow under hypoxic conditions [20]. These authors showed that this effect was mediated by GarA phosphorylation. The proteomic analyses reported here point to the PknG's direct or indirect control of the expression levels of key proteins for hypoxic lifestyle switch as an additional mechanism behind Δ*pknG*'s inability to grow under hypoxia. It is interesting to note that the conserved kinase domain of PknG is flanked by an N-terminal rubredoxin-like domain composed by an iron ion coordinated to four conserved cysteine residues [73,74]. These domains typically participate in electron transfer reactions, and in the case of PknG a role in catalysis regulation has been demonstrated for the rubredoxin-like domain [74]. The possible participation of this rubredoxin like domain in the direct sensing of low oxygen concentrations is an interesting hypothesis to be investigated.

5. Conclusions

Our proteomic data showed that the deletion of *pknG* gene from *M. tuberculosis* causes an alteration in the relative abundance of many proteins that participate in cell envelope biosynthesis, adaptation to hypoxic conditions and the establishment of a persistent bacterial state, in fully agreement with previous functional knowledge about Δ*pknG*. These results, together with previously published data that indicated that PknG sense amino acid availability and regulates glutamate metabolism, allowed us to start delineating a model for PknG's regulation of bacterial adaptation to the nutritional conditions found in the host (Fig. 5). Early macrophage infection studies indicated that deletion of PknG in pathogenic mycobacteria leads to its rapid degradation in mature lysosomes, and suggested that host protein phosphorylation upon PknG secretion could be the mechanism of action [15]. The results presented here support the idea that the direct or indirect regulation of the expression levels of a group of proteins that are relevant for the adaptation of the bacterium to the host environment and the induction of a mycobacterial persistent state might account in part for the effect of PknG on bacterial survival inside the host. Our results reinforce the idea that PknG could represent a very attractive target for the future treatment of tuberculosis, which warrants further studies on its molecular function.

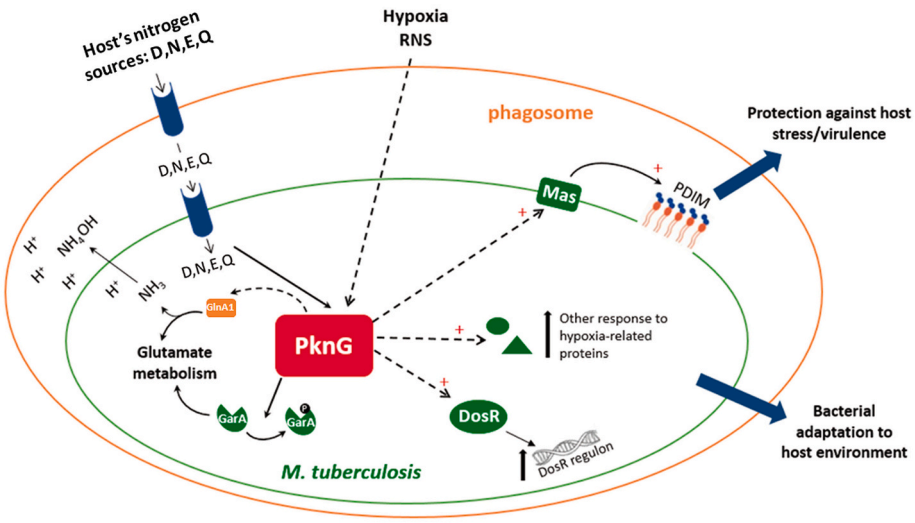

Fig. 5. Model for the role of PknG in bacterial adaptation to nutritional stress inside the host. Previous work demonstrate that PknG regulates glutamate metabolism in mycobacteria through phosphorylation of the GarA protein, and that PknG-GarA signaling pathway plays a key role in *M. tuberculosis*'s ability to survive inside the host [16,17,19,24,75,76]. GarA controls the balance between glutamate synthesis and its oxidative deamination in a phosphorylation-dependent manner. While, unphosphorylated GarA binds to key metabolic enzymes and regulates their activity to promote glutamate synthesis, upon phosphorylation by PknG GarA switches to an inactive conformation favoring glutamate catabolism. More recently we identify Glutamine synthetase (GlnA1) as a putative substrate of this kinase, suggesting a role for PknG in ammonium assimilation regulation through its concerted action on GarA and GlnA1 [24]. PknG responds to nutrient availability, and in particular the amino acids E, D Q and N are the main environmental signals triggering GarA phosphorylation [19]. Interestingly, these amino acids constitute an important source of nitrogen for the bacteria inside host macrophages [77,78]. The results arisen from the present work extend the proposed roles of PknG and allowed us to postulate that this kinase also responds to low oxygen concentration. PknG directly or indirectly regulates the expression levels of the DosR regulon as well as a group of proteins that are considered part of the proteomic hallmark of the hypoxic bacteria. In addition, our results suggest that PknG also controls the levels of key proteins in the biosynthetic pathway of the virulence factor PDIM. Evidence coming from previous results and those arisen from this work allow us to propose a model in which PknG has a central role in redirecting bacterial metabolic flux in response to intracellular environmental stimuli, including host nitrogen sources and hypoxia. Remodeling of bacterial metabolism and cell envelope could be central mechanisms underlying the role of PknG in *M. tuberculosis* growth within host macrophages and virulence.

Supplementary data to this article can be found online at https://doi.org/10.1016/j.jprot.2021.104276.

Declaration of Competing Interest

The authors declare that they have no conflicts of interest with the contents of this article.

Data availability

The mass spectrometry proteomic raw data have been deposited to the ProteomeXchange Consortium *via* the PRIDE partner repository with the dataset identifier PXD023975 for discovery proteomics data and PXD023956 for targeted proteomics data.

Acknowledgments

This work was supported by grants from Agencia Nacional de Investigación e Innovación, Uruguay (ANII, FCE_3_2013_1_100358 and FCE_1_2014_1_104045) and FOCEM - Fondo para la Convergencia Estructural del Mercosur (COF 03/11). MG and BR were supported by fellowships from ANII [POS_NAC_2012_1_8824, POS_NAC_2015_1_109755, POS_FCE_2015_1_1005186]. AC and RB were supported by the Agence Nationale pour la Recherche (France). The authors would like to thank Dr. Av-Gay for kindly providing us with the *M. tuberculosis* Δ*pknG* strain.

References

[1] Global Tuberculosis Report. https://apps.who.int/iris/bitstream/handle/10665/336069/9789240013131-eng.pdf, 2020.
[2] M. Pai, M.A. Behr, D. Dowdy, K. Dheda, M. Divangahi, C.C. Boehme, A. Ginsberg, S. Swaminathan, M. Spigelman, H. Getahun, D. Menzies, M. Raviglione, Tuberculosis, Nat. Rev. Dis. Prim. 2 (2016), https://doi.org/10.1038/nrdp.2016.76.
[3] D.G. Russell, Who puts the tubercle in tuberculosis? Nat. Rev. Microbiol. 5 (2007) 39–47, https://doi.org/10.1038/nrmicro1538.
[4] L.G. Wayne, C.D. Sohaskey, Nonreplicating persistence of *Mycobacterium tuberculosis*, Annu. Rev. Microbiol. 55 (2001) 139–163, https://doi.org/10.1146/annurev.micro.55.1.139.
[5] P.J. Brennan, Structure, function, and biogenesis of the cell wall of *Mycobacterium tuberculosis*, Tuberculosis (Edinb) 83 (2003) 91–97, https://doi.org/10.1016/s1472-9792(02)00089-6.
[6] M. Jackson, The mycobacterial cell envelope–lipids, Cold Spring Harb. Perspect. Med. 4 (2014) a021105, https://doi.org/10.1101/cshperspect.a021105.
[7] A. Sala, P. Bordes, P. Genevaux, Multiple toxin-antitoxin systems in *Mycobacterium tuberculosis*, Toxins (Basel) 6 (2014) 1002–1020, https://doi.org/10.3390/toxins6031002.
[8] B.M. Cumming, J.H. Mazorodze, A.J.C. Steyn, R.M. Wells, D.A. Lamprecht, V. Saini, R.M. Wells, V. Saini, J.H. Mazorodze, A.J.C. Steyn, The physiology and genetics of oxidative stress in mycobacteria, Microbiol. Spect. 2 (2014) 1–22, https://doi.org/10.1128/microbiolspec.MGM2-0019-2013.
[9] A. Bhaskar, C. De Piano, E. Gelman, J.D. McKinney, N. Dhar, Elucidating the role of (p)ppGpp in mycobacterial persistence against antibiotics, IUBMB Life 70 (2018) 1–9, https://doi.org/10.1002/iub.1888.
[10] G. Prosser, J. Brandenburg, N. Reiling, C.E. Barry, R.J. Wilkinson, K.A. Wilkinson, The bacillary and macrophage response to hypoxia in tuberculosis and the consequences for T cell antigen recognition, Microbes Infect. 19 (2017) 177–192, https://doi.org/10.1016/j.micinf.2016.10.001.
[11] S. Lipworth, R.J.H. Hammond, V.O. Baron, Y. Hu, A. Coates, S.H. Gillespie, Defining dormancy in mycobacterial disease, Tuberculosis. 99 (2016) 131–142, https://doi.org/10.1016/j.tube.2016.05.006.
[12] H.-D. Park, K.M. Guinn, M.I. Harrell, R. Liao, M.I. Voskuil, M. Tompa, G. K. Schoolnik, D.R. Sherman, Rv3133c/dosR is a transcription factor that mediates the hypoxic response of *Mycobacterium tuberculosis*, Mol. Microbiol. 48 (2003) 833–843, https://doi.org/10.1046/j.1365-2958.2003.03474.x.
[13] D.M. Roberts, R.P. Liao, G. Wisedchaisri, W.G.J. Hol, D.R. Sherman, Two sensor kinases contribute to the hypoxic response of *Mycobacterium tuberculosis*, J. Biol. Chem. 279 (2004) 23082–23,087, https://doi.org/10.1074/jbc.M401230200.
[14] V. Peddireddy, S.N. Doddam, N. Ahmed, Mycobacterial dormancy systems and host responses in tuberculosis, Front. Immunol. 8 (2017) 1–19, https://doi.org/10.3389/fimmu.2017.00084.
[15] J. Walburger, A. Koul, L. Nguyen, C. Prescianotto-Baschong, K. Huygen, B. Klebl, C. Thompson, C. Bacher, A. Walburger Pieters, A. Koul, G. Ferrari, L. Nguyen, C. Prescianotto-Baschong, K. Huygen, B. Klebl, C. Thompson, G. Bacher, J. Pieters, Protein kinase G from pathogenic mycobacteria promotes survival within macrophages, Science. 304 (2004) 1800–1804, https://doi.org/10.1126/science.1099384.
[16] M. Ventura, B. Rieck, F. Boldrin, G. Degiacomi, M. Bellinzoni, N. Barilone, F. Alzaidi, P.M. Alzari, R. Manganelli, H.M. O'Hare, GarA is an essential regulator of metabolism in *Mycobacterium tuberculosis*, Mol. Microbiol. 90 (2013) 356–366, https://doi.org/10.1111/mmi.12368.
[17] H.M. O'Hare, R. Durán, C. Cerveñansky, M. Bellinzoni, A.M. Wehenkel, O. Pritsch, G. Obal, J. Baumgartner, J. Vialaret, K. Johnsson, P.M. Alzari, Regulation of glutamate metabolism by protein kinases in mycobacteria, Mol. Microbiol. 70 (2008) 1408–1423, https://doi.org/10.1111/j.1365-2958.2008.06489.x.
[18] S. Cowley, M. Ko, N. Pick, R. Chow, K.J. Downing, B.G. Gordhan, J.C. Betts, V. Mizrahi, D. Smith, R.W. Stokes, Y. Av-Gay, The *Mycobacterium tuberculosis*

protein serine/threonine kinase PknG is linked to cellular glutamate/glutamine levels and is important for growth *in vivo*, Mol. Microbiol. 52 (2004) 1691–1702, https://doi.org/10.1111/j.1365-2958.2004.04085.x.
[19] B. Rieck, G. Degiacomi, M. Zimmermann, A. Cascioferro, F. Boldrin, N.R. Lazar-Adler, A.R. Bottrill, F. le Chevalier, W. Frigui, M. Bellinzoni, M.-N.N. Lisa, P. M. Alzari, L. Nguyen, R. Brosch, U. Sauer, R. Manganelli, H.M. O'Hare, H. M. O'Hare, PknG senses amino acid availability to control metabolism and virulence of *Mycobacterium tuberculosis*, PLoS Pathog. 13 (2017), e1006399, https://doi.org/10.1371/journal.ppat.1006399.
[20] M.Z. Khan, A. Bhaskar, S. Upadhyay, P. Kumari, R.S. Rajmani, P. Jain, A. Singh, D. Kumar, N.S. Bhavesh, V.K. Nandicoori, Protein kinase G confers survival advantage to *Mycobacterium tuberculosis* during latency-like conditions, J. Biol. Chem. 292 (2017) 16093–16108, https://doi.org/10.1074/jbc.M117.797563.
[21] R. Paroha, R. Chourasia, R. Mondal, S.K. Chaurasiya, PknG supports mycobacterial adaptation in acidic environment, Mol. Cell. Biochem. (2017) 1–12, https://doi.org/10.1007/s11010-017-3211-x.
[22] K.A. Wolff, H.T. Nguyen, R.H. Cartabuke, A. Singh, S. Ogwang, L. Nguyen, Protein kinase G is required for intrinsic antibiotic resistance in mycobacteria, Antimicrob. Agents Chemother. 53 (2009) 3515–3519, https://doi.org/10.1128/AAC.00012-09.
[23] K.A. Wolff, A.H. de la Peña, H.T. Nguyen, T.H. Pham, L.M. Amzel, S.B. Gabelli, L. Nguyen, A redox regulatory system critical for mycobacterial survival in macrophages and biofilm development, PLoS Pathog. 11 (2015) 1–20, https://doi.org/10.1371/journal.ppat.1004839.
[24] M. Gil, A. Lima, B. Rivera, J. Rossello, E. Urdániz, F. Carrión, A. Wehenkel, M. Bellinzoni, C. Batthyány, A. Denicola, M.N. Alvarez, M.-N.N. Lisa, R. Brosch, M. Piuri, P.M. Alzari, R. Durán, New substrates and interactors of the mycobacterial Serine/Threonine protein kinase PknG identified by a tailored interactomic approach, J. Proteome 192 (2018) 321–333, https://doi.org/10.1016/J.JPROT.2018.09.013.
[25] K.C. Nakedi, B. Calder, M. Barnejee, A. Giddey, A.J. Nel, S. Garnett, J. M. Blackburn, N.A. Soares, Identification of novel physiological substrates of *Mycobacterium bovis* BCG Protein Kinase G (PknG) by label-free quantitative phosphoproteomics, Mol. Cell. Proteomics (2018), https://doi.org/10.1074/mcp.RA118.000705 (mcp.RA118.000705).
[26] F.-L. Wu, Y. Liu, H. Jiang, Y.-Z. Luan, H. Zhang, X. He, Z.-W. Xu, J.-L. Hou, L.-Y. Ji, Z. Xie, D.M. Czajkowsky, W. Yan, J.-Y. Deng, L.-J. Bi, X.-E. Zhang, S.-C. Tao, The Ser/Thr protein kinase protein-protein interaction map of *M. tuberculosis*, Mol. Cell. Proteomics 16 (2017) 1491–1506, https://doi.org/10.1074/mcp.M116.065771.
[27] S.S. Baros, J.M. Blackburn, N.C. Soares, Phosphoproteomic approaches to discover novel substrates of mycobacterial Ser/Thr protein kinases, Mol. Cell. Proteomics 19 (2020) 233–244, https://doi.org/10.1074/mcp.R119.001668.
[28] G.E. Healthcare, Amersham CyDye DIGE Fluors (minimal dyes) for 2D DIGE, Gen. Electr. Co., 2002, pp. 1–28. http://www.gelifesciences.com.
[29] A. Gorg, 2-D Electrophoresis. Principles and Methods, Handbook, 2004, p. 163, https://doi.org/10.1186/1755-8794-4-24.
[30] GE Healthcare, Typhoon TM FLA 7000 Biomolecular Imager, 2009, pp. 1–6.
[31] A. Shevchenko, M. Wilm, O. Vorm, M. Mann, Mass spectrometric sequencing of proteins from silver-stained polyacrylamide gels mass spectrometric sequencing of proteins from silver-stained polyacrylamide gels, Anal. Chem. 68 (1996) 850–858, https://doi.org/10.1021/ac950914h.
[32] A. Lima, R. Durán, G.E. Schujman, M.J. Marchissio, M.M. Portela, G. Obal, O. Pritsch, D. de Mendoza, C. Cerveñansky, Serine/threonine protein kinase PrkA of the human pathogen *Listeria monocytogenes*: biochemical characterization and identification of interacting partners through proteomic approaches, J. Proteome 74 (2011) 1720–1734, https://doi.org/10.1016/j.jprot.2011.03.005.
[33] P.C. Carvalho, D.B. Lima, F.V. Leprevost, M.D.M. Santos, J.S.G. Fischer, P. F. Aquino, J.J. Moresco, J.R. Yates, V.C. Barbosa, J.R.Y. Iii, V.C. Barbosa, Integrated analysis of shotgun proteomic data with PatternLab for proteomics 4.0, Nat. Protoc. 11 (2016) 102–117, https://doi.org/10.1038/nprot.2015.133.
[34] P.C. Carvalho, J.S.G. Fischer, J. Perales, J.R. Yates, V.C. Barbosa, E. Bareinboim, Analyzing marginal cases in differential shotgun proteomics, Bioinformatics. 27 (2011) 275–276, https://doi.org/10.1093/bioinformatics/btq632.
[35] H. Mi, S. Poudel, A. Muruganujan, J.T. Casagrande, P.D. Thomas, PANTHER version 10: Expanded protein families and functions, and analysis tools, Nucleic Acids Res. 44 (2016) D336–D342, https://doi.org/10.1093/nar/gkv1194.
[36] Y. Perez-Riverol, A. Csordas, J. Bai, M. Bernal-Llinares, S. Hewapathirana, D. J. Kundu, A. Inuganti, J. Griss, G. Mayer, M. Eisenacher, E. Pérez, J. Uszkoreit, J. Pfeuffer, T. Sachsenberg, Ş. Yilmaz, S. Tiwary, J. Cox, E. Audain, M. Walzer, A. F. Jarnuczak, T. Ternent, A. Brazma, J.A. Vizcaíno, The PRIDE database and related tools and resources in 2019: improving support for quantification data, Nucleic Acids Res. 47 (2019) D442–D450, https://doi.org/10.1093/nar/gky1106.
[37] M. Gengenbacher, J. Mouritsen, O.T. Schubert, R. Aebersold, S.H.E. Kaufmann, *Mycobacterium tuberculosis* in the proteomics Era, Microbiol. Spect. 2 (2014), https://doi.org/10.1128/microbiolspec.MGM2-0020-2013.
[38] R. Pandey, G.M. Rodriguez, A ferritin mutant of *Mycobacterium tuberculosis* is highly susceptible to killing by antibiotics and is unable to establish a chronic infection in mice, Infect. Immun. 80 (2012) 3650–3659, https://doi.org/10.1128/IAI.00229-12.
[39] P.V. Reddy, R.V. Puri, A. Khera, A.K. Tyagi, Iron storage proteins are essential for the survival and pathogenesis of *Mycobacterium tuberculosis* in THP-1 macrophages and the guinea pig model of infection, J. Bacteriol. 194 (2012) 567–575, https://doi.org/10.1128/JB.05553-11.
[40] V. Sharma, S. Sharma, K. Hoener zu Bentrup, J.D. McKinney, D.G. Russell, W. R. Jacobs, J.C. Sacchettini, Structure of isocitrate lyase, a persistence factor of *Mycobacterium tuberculosis*, Nat. Struct. Biol. 7 (2000) 663–668, https://doi.org/10.1038/77964.
[41] M.M. Giffin, L. Shi, M.L. Gennaro, C.D. Sohaskey, Role of alanine dehydrogenase of *Mycobacterium tuberculosis* during recovery from hypoxic nonreplicating persistence, PLoS One 11 (2016) 1–18, https://doi.org/10.1371/journal.pone.0155522.
[42] A. Luthra, S.S. Malik, R. Ramachandran, Cloning, purification and comparative structural analysis of two hypothetical proteins from *Mycobacterium tuberculosis* found in the human granuloma during persistence and highly up-regulated under carbon-starvation conditions, Protein Expr. Purif. 62 (2008) 64–74, https://doi.org/10.1016/j.pep.2008.06.011.
[43] E.S.V. Andrews, V.L. Arcus, The mycobacterial PhoH2 proteins are type II toxin antitoxins coupled to RNA helicase domains, Tuberculosis 95 (2015) 385–394, https://doi.org/10.1016/j.tube.2015.03.013.
[44] S. Selvaraj, V. Sambandam, D. Sardar, S. Anishetty, *In silico* analysis of DosR regulon proteins of *Mycobacterium tuberculosis*, Gene. 506 (2012) 233–241, https://doi.org/10.1016/j.gene.2012.06.033.
[45] I. Keren, S. Minami, E. Rubin, K.C. Lewis, Characterization and transcriptome analysis of *Mycobacterium tuberculosis* persisters, MBio. 2 (2011), e00100-11, https://doi.org/10.1128/mBio.00100-11.
[46] M. Gengenbacher, S.H. Kaufmann, *Mycobacterium tuberculosis*: success through dormancy, FEMS Microbiol. Rev. 36 (2012) 514–532, https://doi.org/10.1111/j.1574-6976.2012.00331.x.
[47] G.M. Rodriguez, M.I. Voskuil, B. Gold, G.K. Schoolnik, I. Smith, ideR, An essential gene in *Mycobacterium tuberculosis*: role of IdeR in iron-dependent gene expression, iron metabolism, and oxidative stress response, Infect. Immun. 70 (2002) 3371–3381, https://doi.org/10.1128/iai.70.7.3371-3381.2002.
[48] B. Gold, G.M. Rodriguez, S.A. Marras, M. Pentecost, I. Smith, The *Mycobacterium tuberculosis* IdeR is a dual functional regulator that controls transcription of genes involved in iron acquisition, iron storage and survival in macrophages, Mol. Microbiol. 42 (2001) 851–865, https://doi.org/10.1046/j.1365-2958.2001.02684.x.
[49] M.Z. Khan, V.K. Nandicoori, Deletion of PknG abates reactivation of latent *Mycobacterium tuberculosis* in mice, Antimicrob. Agents Chemother. (2021), https://doi.org/10.1128/aac.02095-20.
[50] G. Pradhan, R. Shrivastva, S. Mukhopadhyay, Mycobacterial PknG targets the Rab7l1 signaling pathway to inhibit phagosome–lysosome fusion, J. Immunol. 201 (2018) 1421–1433, https://doi.org/10.4049/jimmunol.1800530.
[51] J. Plumbridge, Regulation of the utilization of amino sugars by *Escherichia coli* and *Bacillus subtilis*: same genes, different control, J. Mol. Microbiol. Biotechnol. 25 (2015) 154–167, https://doi.org/10.1159/000369583.
[52] C. Kang, D.W. Abbott, S.T. Park, C.C. Dascher, L.C. Cantley, R.N. Husson, The *Mycobacterium tuberculosis* serine/threonine kinases PknA and PknB: substrate identification and regulation of cell shape, Genes Dev. 19 (2005) 1692–1704, https://doi.org/10.1101/gad.1311105.nism.
[53] M. Bellinzoni, A.M. Wehenkel, R. Durán, P.M. Alzari, Novel mechanistic insights into physiological signaling pathways mediated by mycobacterial Ser/Thr protein kinases, Genes Immun. (2019), https://doi.org/10.1038/s41435-019-0069-9.
[54] L.E.N. Quadri, Biosynthesis of mycobacterial lipids by polyketide synthases and beyond, Crit. Rev. Biochem. Mol. Biol. 49 (2014) 179–211, https://doi.org/10.3109/10409238.2014.896859.
[55] D.L. Rainwater, P.E. Kolattukudy, Fatty acid biosynthesis in *Mycobacterium tuberculosis* var. bovis Bacillus Calmette-Guérin. Purification and characterization of a novel fatty acid synthase, mycocerosic acid synthase, which elongates n-fatty acyl-CoA with methylmalonyl-CoA, J. Biol. Chem. 260 (1985) 616–623.
[56] A.K. Azad, T.D. Sirakova, D. Norvin, P.E. Kolattukudy, Gene Knockout Reveals a Novel Gene Cluster for the Synthesis of a Class of Cell Wall Lipids Unique to Pathogenic Mycobacteria Gene Knockout Reveals a Novel Gene Cluster for the Synthesis of a Cl vol. 272, 1997, pp. 16741–16745, https://doi.org/10.1074/jbc.272.27.16741.
[57] V.S. Dubey, T.D. Sirakova, P.E. Kolattukudy, Disruption of msl3 abolishes the synthesis of mycolipanoic and mycolipenic acids required for polyacyltrehalose synthesis in *Mycobacterium tuberculosis* H37Rv and causes cell aggregation, Mol. Microbiol. 45 (2002) 1451–1459, https://doi.org/10.1046/j.1365-2958.2002.03119.x.
[58] M.S. Li, I.M. Monahan, S.J. Waddell, J.A. Mangan, S.L. Martin, M.J. Everett, P. D. Butcher, cDNA-RNA subtractive hybridization reveals increased expression of mycocerosic acid synthase in intracellular *Mycobacterium bovis* BCG, Microbiology. 147 (2001) 2293–2305, https://doi.org/10.1099/00221287-147-8-2293.
[59] M. Jackson, G. Stadthagen, B. Gicquel, Long-chain multiple methyl-branched fatty acid-containing lipids of *Mycobacterium tuberculosis*: biosynthesis, transport, regulation and biological activities, Tuberculosis. 87 (2007) 78–86, https://doi.org/10.1016/j.tube.2006.05.003.
[60] M.B. Goren, O. Brokl, W.B. Schaefer, Lipids of putative relevance to virulence in *Mycobacterium tuberculosis*: phthiocerol dimycocerosate and the attenuation indicator lipid, Infect. Immun. 9 (1974) 150–158, https://doi.org/10.1128/iai.9.1.150-158.1974.

[61] K. Pethe, D.L. Swenson, S. Alonso, J. Anderson, C. Wang, D.G. Russell, Isolation of *Mycobacterium tuberculosis* mutants defective in the arrest of phagosome maturation, Proc. Natl. Acad. Sci. U. S. A. 101 (2004) 13642–13647, https://doi.org/10.1073/pnas.0401657101.

[62] C. Rousseau, N. Winter, E. Privert, Y. Bordat, O.O. Neyrolles, P. Avé, M. Huerre, B. Gicquel, M. Jackson, E. Pivert, Y. Bordat, O.O. Neyrolles, P. Avé, M. Huerre, B. Gicquel, M. Jackson, Production of phthiocerol dimycocerosates protects *Mycobacterium tuberculosis* from the cidal activity of reactive nitrogen intermediates produced by macrophages and modulates the early immune response to infection, Cell. Microbiol. 6 (2004) 277–287, https://doi.org/10.1046/j.1462-5822.2004.00368.x.

[63] J. Quigley, V.K. Hughitt, C.A. Velikovsky, R.A. Mariuzza, N.M. El-Sayed, V. Briken, The cell wall lipid PDIM contributes to phagosomal escape and host cell exit of *Mycobacterium tuberculosis*, MBio 8 (2017), https://doi.org/10.1128/mBio.00148-17.

[64] I. Rosenkrands, R.A. Slayden, J. Crawford, C. Aagaard, C.E. Barry, P. Andersen, Hypoxic response of *Mycobacterium tuberculosis* studied by metabolic labeling and proteome analysis of cellular and extracellular proteins, J. Bacteriol. 184 (2002) 3485–3491, https://doi.org/10.1128/jb.184.13.3485-3491.2002.

[65] D.R. Sherman, M. Voskuil, D. Schnappinger, R. Liao, M.I. Harrell, G.K. Schoolnik, Regulation of the *Mycobacterium tuberculosis* hypoxic response gene encoding alpha -crystallin, Proc. Natl. Acad. Sci. U. S. A. 98 (2001) 7534–7539, https://doi.org/10.1073/pnas.121172498.

[66] C. Boon, T. Dick, Mycobacterium bovis BCG response regulator essential for hypoxic dormancy, J. Bacteriol. 184 (2002) 6760–6767, https://doi.org/10.1128/jb.184.24.6760-6767.2002.

[67] Y. Hu, F. Movahedzadeh, N.G. Stoker, A.R.M. Coates, Deletion of the *Mycobacterium tuberculosis* α-crystallin-like hspX gene causes increased bacterial growth *in vivo*, Infect. Immun. 74 (2006) 861–868, https://doi.org/10.1128/IAI.74.2.861-868.2006.

[68] M.L. Sharpe, C. Gao, S.L. Kendall, E.N. Baker, J.S. Lott, The structure and unusual protein chemistry of hypoxic response protein 1, a latency antigen and highly expressed member of the DosR regulon in *Mycobacterium tuberculosis*, J. Mol. Biol. 383 (2008) 822–836, https://doi.org/10.1016/j.jmb.2008.07.001.

[69] J. Bi, Y. Wang, H. Yu, X. Qian, H. Wang, J. Liu, X. Zhang, Modulation of central carbon metabolism by acetylation of isocitrate lyase in *Mycobacterium tuberculosis*, Sci. Rep. 7 (2017), https://doi.org/10.1038/srep44826.

[70] H.J. Bae, H.N. Lee, M.N. Baek, E.J. Park, C.Y. Eom, I.J. Ko, H.Y. Kang, J. Il Oh, Inhibition of the devSR two-component system by overexpression of *Mycobacterium tuberculosis* PknB in *Mycobacterium smegmatis*, Mol. Cell 40 (2017) 632–642, https://doi.org/10.14348/molcells.2017.0076.

[71] B.D. Parthiban, S. Saxena, M. Chandran, P.S. Jonnalagadda, R. Yadav, R. R. Srilakshmi, Y. Perumal, S. Dharmarajan, Design and development of *Mycobacterium tuberculosis* lysine ε -aminotransferase inhibitors for latent tuberculosis infection, Chem. Biol. Drug Des. 87 (2016) 265–274, https://doi.org/10.1111/cbdd.12655.

[72] J.C. Betts, P.T. Lukey, L.C. Robb, R.A. McAdam, K. Duncan, Evaluation of a nutrient starvation model of *Mycobacterium tuberculosis* persistence by gene and protein expression profiling, Mol. Microbiol. 43 (2002) 717–731, https://doi.org/10.1046/j.1365-2958.2002.02779.x.

[73] N. Scherr, S. Honnappa, G. Kunz, P. Mueller, R. Jayachandran, F. Winkler, J. Pieters, M.O. Steinmetz, Structural basis for the specific inhibition of protein kinase G, a virulence factor of *Mycobacterium tuberculosis*, Proc. Natl. Acad. Sci. U. S. A. 104 (2007) 12151–12156, https://doi.org/10.1073/pnas.0702842104.

[74] M.N. Lisa, M. Gil, G. André-Leroux, N. Barilone, R. Durán, R.M. Biondi, P.M. Alzari, Molecular basis of the activity and the regulation of the eukaryotic-like S/T protein kinase PknG from *Mycobacterium tuberculosis*, Structure. 23 (2015) 1039–1048, https://doi.org/10.1016/j.str.2015.04.001.

[75] N. Bhattacharyya, N. Nkumama, Z. Newland-smith, L. Lin, W. Yin, R.E. Cullen, J. S. Cullen, A.R. Jarvis, M.J. Price, P.Y. Chong, R. Wallis, H.M. O'Hare, An aspartate-specific solute-binding protein regulates protein Kinase G activity to control glutamate metabolism in mycobacteria, mBio (2018), e00931-18, https://doi.org/10.1128/mBio.00931-18.

[76] M. Bellinzoni, A.M. Wehenkel, R. Durán, P.M. Alzari, Novel mechanistic insights into physiological signaling pathways mediated by mycobacterial Ser/Thr protein kinases, Genes Immun. 20 (2019) 383–393, https://doi.org/10.1038/s41435-019-0069-9.

[77] K. Borah, M. Beyß, A. Theorell, H. Wu, P. Basu, T.A. Mendum, K. Nöh, D.J.V. Beste, J. McFadden, Intracellular *Mycobacterium tuberculosis* exploits multiple host nitrogen sources during growth in human macrophages, Cell Rep. 29 (2019) 3580–3591.e4, https://doi.org/10.1016/j.celrep.2019.11.037.

[78] A. Gouzy, G. Larrouy-Maumus, D. Bottai, F. Levillain, A. Dumas, J.B. Wallach, I. Caire-Brandli, C. de Chastellier, T.D. Wu, R. Poincloux, R. Brosch, J.L. Guerquin-Kern, D. Schnappinger, L.P. Sório de Carvalho, Y. Poquet, O. Neyrolles, *Mycobacterium tuberculosis* exploits asparagine to assimilate nitrogen and resist acid stress during infection, PLoS Pathog. 10 (2014), e1003928, https://doi.org/10.1371/journal.ppat.1003928.